ISSN 1392-3730/eISSN 1822-3605

VILNIUS TECH
Vilnius Gediminas Technical University

JOURNAL of CIVIL ENGINEERING and MANAGEMENT

2024
Volume 30
Issue 3
Pages 264–278
https://doi.org/10.3846/jcem.2024.20778

BACK ANALYSIS AND STABILITY PREDICTION OF SURROUNDING ROCK DURING EXCAVATION OF THE SHUANGJIANGKOU UNDERGROUND POWERHOUSE

You LI[1], Ming-Li XIAO[1], Gan FENG[1]✉, Ming-Guang CAI[2], Jia-Ming WU[1], Jian-Liang PEI[1], Jiang-Da HE[1]

[1] *State Key Laboratory of Hydraulics and Mountain River Engineering, College of Water Resource and Hydropower, Sichuan University, Chengdu, China*
[2] *Sinohydro Bureau 7 Co., LTD, Chengdu, China*

Article History:
- received 26 September 2023
- accepted 13 November 2023

Abstract. The underground powerhouse of the Shuangjiangkou hydropower station is one of the largest caverns under construction in China, and its stability during construction is crucial for safe construction. To study the stability of the surrounding rock during excavation, the displacement and stress of the surrounding rock were monitored by multi-point displacement meters and bolt stress meters. Based on the monitoring data, the elastic modulus, Poisson's ratio, friction angle, and cohesion of surrounding rock were inversely analyzed by the PSO-BP algorithm. Then, the back-analyzed parameters were used to simulate the subsequent excavations and predict the stability of surrounding rock during the following construction. The analysis results show that the surrounding rocks were generally stable during the initial four stages of excavation, and the main factors affecting their stability were blasts and unfavorable geological structures, including the lamprophyre vein and the F1 fault. These unfavorable geological structures also significantly decrease the mechanical parameters of surrounding rock as demonstrated by back analysis, and the stability prediction results show that the omnibus bar cave and the tailrace tunnel were at the greatest risk of instability during the subsequent excavations. This study provides a practical analysis for engineering excavation of the underground caverns.

Keywords: underground cavern, back analysis, stability prediction, safety monitoring, neural network algorithm, numerical simulation.

✉Corresponding author. E-mail: *fenggan@scu.edu.cn*

1. Introduction

The stability of rock masses surrounding an underground powerhouse is very crucial during its construction and has widely got engineers' attention (Zheng et al., 2018). The underground caverns of the hydropower station are usually located in a complex geological environment. The stability of these caverns is affected by various factors, such as mechanical properties of surrounding rock (He et al., 2021; Sudhakar et al., 2023; Sun et al., 2023), in-situ stress (Moomivand et al., 2022; Sainoki et al., 2020; Zhang et al., 2021), unfavorable geological structure (Kuili & Sastry, 2023; Ma et al., 2020a; Prajapati & Verma, 2023), underground water (Li et al., 2014; Xu et al., 2020), and excavation method (Chandra et al., 2010; Ma et al., 2023; Rahimi et al., 2021). Due to the uncertainty of geological conditions, it is not easy to obtain all details of geological and environmental factors. Thus, to ensure the stability of underground powerhouse during the construction and operation, it is essential to monitor the deformation and stress of surrounding rock masses.

Currently, the monitoring methods of surrounding rock's safety during the construction of underground caverns mainly include conventional monitoring technique (Ding & Qin, 2000; Hanna, 1985; Mikolas et al., 2021) (such as multi-point displacement meter, bolt stress meter, anchor cable stress meter, etc.), acoustic emission monitoring technique (Gholizadeh et al., 2015; Manthei & Plenkers, 2018; Ono, 2018), microseismic monitoring technique (Blake, 1974; Warpinski, 2009; Zhao et al., 2014), fiber optic sensor monitoring technique (Choi et al., 2016; Gong et al., 2019), and space monitoring technique (Bacova et al., 2021; Lechner & Baumann, 2000; Yu et al., 2020), etc. For example, Małkowski et al. (2021) introduced an automatic monitoring system composed of several monitoring devices, such as rod extensometer, rock bolt stress meter,

and biaxial stress meter, and successfully applied it to the maingate PW-1 in "Pniówek" coal mine. Sun et al. (2021) applied acoustic emission and stress monitoring techniques to the surrounding rock of the Gaoloushan tunnel and proposed a warning method for potential destructive disasters. Kumar et al. (2021) evaluated the dynamic stability of the underground powerhouse of the Tala hydropower plant using microseismic monitoring and concluded that no major earthquake events would occur around the cavern. Lanciano et al. (2021) established a fiber optic sensor monitoring system to measure the strain and temperature of an underground marble quarry in Italy.

Numerical simulation is also an important method for analyzing the stability of surrounding rock. Dhawan et al. (2004) carried out finite element simulation on rock deformation around the underground powerhouse of the Koyna hydropower station in India and verified the simulation results with on-site measurements. Ma et al. (2020b) and Qian and Zhou (2018) combined finite element simulation and in-situ monitoring to analyze the rock deformation and damage mechanism of surrounding rock during the excavations of the underground powerhouse of the Jinping I hydropower station. Khayrutdinov et al. (2021) employed the FLAC3D software to study the stress-strain state of underground mining systems, and proposed a differentiated method which can be used to evaluate the state of rock masses. Ma et al. (2016) put forward a stability analysis method for underground caverns that combines numerical simulation and microseismic monitoring, and successfully applied it to an underground sealed storage cavern. Vo et al. (2022) utilized numerical methods to evaluate the stability of an underground cavern in Vietnam. Sari (2022) used the finite element method to analyze the two- and three-dimensional stability of underground storage caverns in the soft rock of Cappadocia, Turkey, and found that 15 m seems to be the best depth for digging typical underground storage caverns. Rezaei and Rajabi (2018) used numerical analysis to predict the vertical displacement of the roof and floor of the powerhouse cavern under different conditions. Rajabi et al. (2021) proposed an optimum equation to predict the deformation of surrounding rock of the underground powerhouse by using gene expression programming and numerical simulation. Ma et al. (2017) proposed an effective method to analyze the stability and reinforcement effect of the Dagangshan rock slope and validated it with numerical simulations. Menéndez et al. (2020) conducted three-dimensional numerical simulations to verify the stability of an underground pumped storage hydropower station in Spain and evaluated the deformation and thickness of the excavation damage zone around the excavation.

Analyzing the above, it can be noted that the stability analysis of surrounding rock during the excavation of underground caverns is a very topical issue. However, for the Shuangjiangkou underground powerhouse, which is one of the largest underground caverns in the world, there are few studies to inversely analyze the mechanical parameters and the stability of its surrounding rock based on the monitoring data during its construction. Therefore, the purpose of this study is to present a complete and cyclable analysis process of on-site monitoring, back analysis, and stability prediction and to demonstrate the feasibility and practicability of the entire process by a new engineering application. To achieve this, it is necessary to solve the following tasks: 1) The deformation and stress characteristics of the rock mass surrounding the Shuangjiangkou underground powerhouse, which is still under construction, during the initial four layers of excavation need to be analyzed; 2) The mechanical parameters of the surrounding rock need to be inversely analyzed based on the particle swarm optimization back propagation (PSO-BP) neural network algorithm; 3) The back-analyzed parameters need to be substituted into the established numerical model to predict the mechanical responses and stability of surrounding rock masses during the subsequent excavations.

2. Engineering background

2.1. Engineering geology

The Shuangjiangkou hydropower station is located in Jinchuan County, Aba Tibetan and Qiang Autonomous Prefecture, Sichuan Province, China. Its underground powerhouse is located on the left abutment of the dam and the upstream side of the dam's axis. The total length of the main powerhouse is 219.48 m. The minimum horizontal buried depth is about 400 m, and the vertical buried depth is about 320 m to 500 m. The main powerhouse includes three parts: the main machine room, the auxiliary powerhouse, and the installation room. The installation room and the auxiliary powerhouse are located at two ends of the main powerhouse. In the main machine room, the span of the top arch is 28.30 m, the maximum excavation height is 68.32 m, and the length is 135.06 m. In the installation room, the span of the top arch is 28.30 m, the maximum excavation height is 29.22 m, and the length is 54.02 m. In the auxiliary powerhouse, the span of the top arch is 25.30 m, the maximum excavation height is 42.72 m, and the length is 30.40 m.

The stratum lithology around the underground powerhouse is mainly porphyritic biotite K-feldspar granite, and the rock mass is fresh and hard. There are some granitic pegmatite veins and a few fine-grained veins in surrounding rock. Especially, a lamprophyre vein and a local small fault cross the underground powerhouse, and both unfavorable geological structures will affect the integrity, strength, and stability of surrounding rock. The surrounding rock has good integrity, and its structure presents as a large block structure. The wall of the exploration tunnel is dry, and seepage, drip water, and slight flowing water were observed in a few tunnel sections. Thus, most of the surrounding rocks are classified as class IIIa, and the surrounding rocks near the fault and lamprophyre vein are classified as class IV to V in the geological survey report of the Shuangjiangkou hydropower station.

2.2. Layout of monitoring instruments

Some monitoring instruments including multi-point displacement meters and bolt stress meters are equipped in six monitoring sections of the Shuangjiangkou underground powerhouse, as shown in Figure 1. These monitoring sections have the chainages of 0 – 52.32 m, 0 + 0.00 m, 0 + 30.02 m, 0 + 60.04 m, 0 + 90.06 m, and 0 + 135.00 m, respectively.

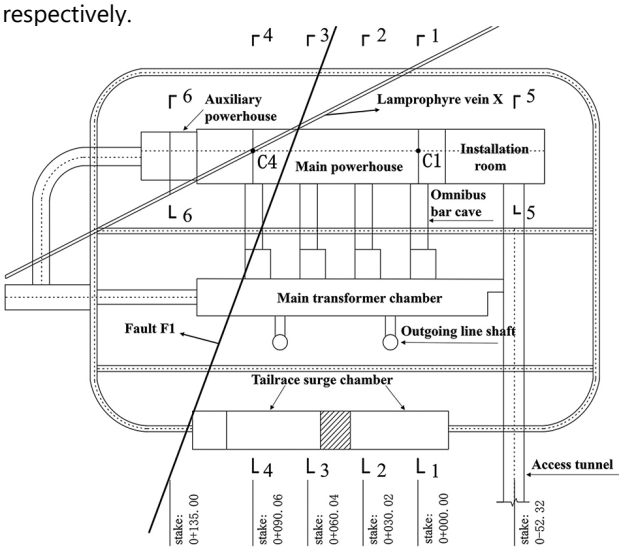

Figure 1. Monitoring sections of the underground powerhouse in the Shuangjiangkou hydropower station

Sections 1-1, 2-2, 3-3, and 4-4 are perpendicular to the axis of the main powerhouse and along the axis of 1#~4# electric generators in the main machine room, respectively, and these sections also traverse the omnibus bar cave, the main transformer chamber, the tailrace tunnel, and then tailrace surge chamber. Sections 5-5 and 6-6 are the monitoring sections in the installation room and the auxiliary powerhouse, respectively.

The layout of monitoring instruments in these monitoring sections is almost the same. The monitoring instruments are mainly installed on the vault, spandrel, rock anchor beam, and sidewall of the underground powerhouse. Multi-point displacement meter and bolt stress meter are two kinds of main monitoring instruments, and their layouts in the section of the 1# electric generator are shown in Figure 2 and Figure 3, respectively.

As of March 2022, four layers of excavation have been completed in the Shuangjiangkou underground powerhouse, as shown in Figure 4. Only some of monitoring instruments have been installed because the underground powerhouse is still under construction. 52 sets of multi-point displacement meters and 35 sets of bolt stress meters have been installed in the main powerhouse. The amount of these monitoring instruments is almost 80% of the total amount, and the details of these installed monitoring instruments are listed in Table 1.

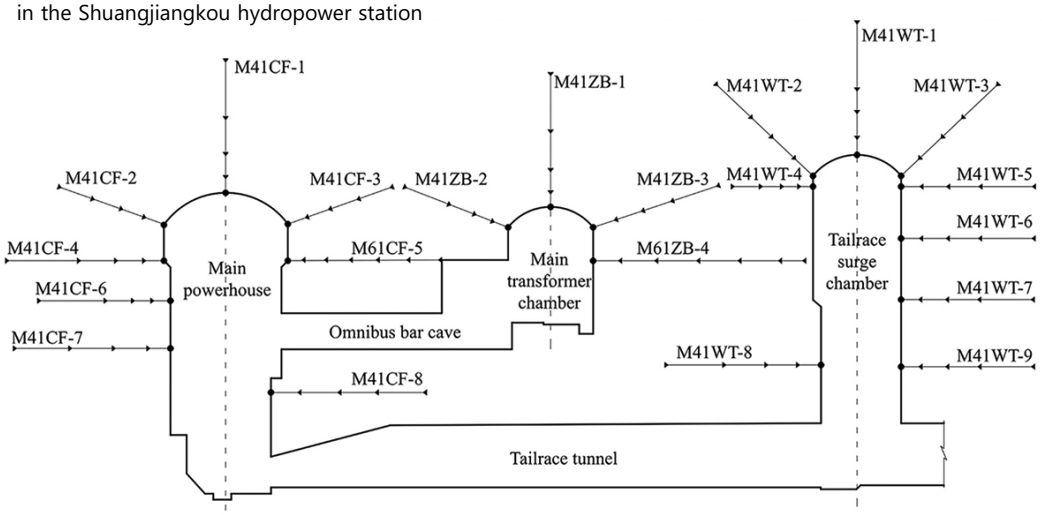

Figure 2. Layout of multi-point displacement meters in the section of the 1# electric generator

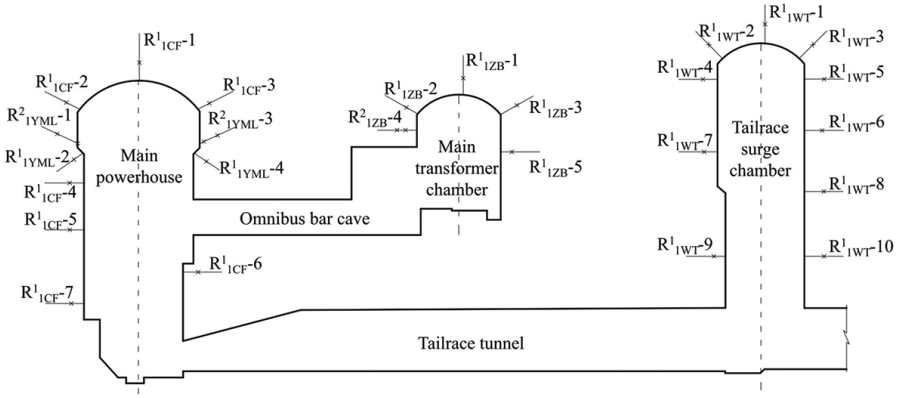

Figure 3. Layout of bolt stress meters in the section of the 1# electric generator

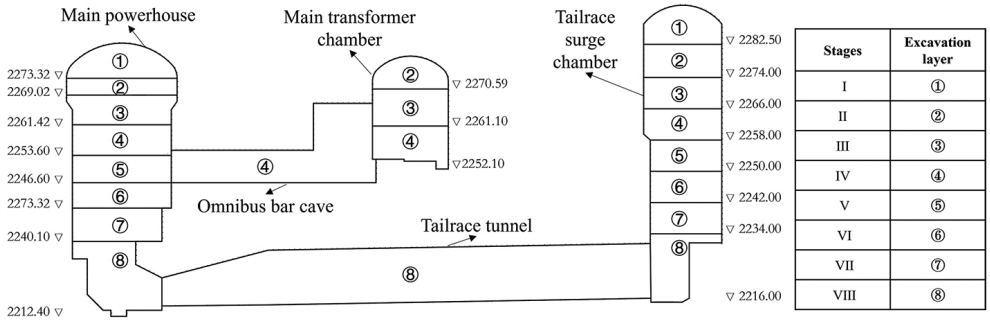

Figure 4. Excavation scheme of the underground powerhouse in the Shuangjiangkou hydropower station

Table 1. Details of the installed monitoring instruments in the underground powerhouse

No.	Instrument name	Specification	Quantity (set)
1	Four-point displacement meter	Vibrating wire type, Measure range: 100 mm, resolution ≤ 0.025% FS	97
2	Four-point displacement meter	Vibrating wire type, Measure range: 200 mm, resolution ≤ 0.025% FS	11
3	Six-point displacement meter	Vibrating wire type, Measure range: 100 mm, resolution ≤ 0.025% FS	11
4	Six-point displacement meter	Vibrating wire type, Measure range: 200 mm, resolution ≤ 0.025% FS	6
5	Single-point bolt stress meter	Differential resistance type, ϕ 32, Measure range: –100 MPa~400 MPa, resolution ≤ 0.30% FS	20
6	Single-point bolt stress meter	Differential resistance type, ϕ 64, Measure range: –100 MPa~400 MPa, resolution ≤ 0.30% FS	110
7	Two-point bolt stress meter	Differential resistance type, ϕ 32, Measure range: –100 MPa~400 MPa, resolution ≤ 0.30% FS	3
8	Two-point bolt stress meter	Differential resistance type, ϕ 64, Measure range: –100 MPa~400 MPa, resolution ≤ 0.30% FS	10

3. Monitoring data analysis

Due to the vast scale of the Shuangjiangkou underground powerhouse, its monitoring system is complex, and the monitoring type and data are enormous. Thus, we focus on analyzing the monitoring data of multi-point displacement meters and bolt stress meters in the main powerhouse.

3.1. Analysis of monitoring data measured by multi-point displacement meters

To illustrate the deformation process of surrounding rock during excavation of the main powerhouse, six of these multi-point displacement meters in the section of the 1# electric generator, and their monitoring data are taken as an example and presented here. Their positions are shown in Figure 2. The M41CF-01 multi-point displacement meter was installed after excavating the pilot tunnel of the main powerhouse. The M41CF-02 and M41CF-03 multi-point displacement meters were installed from the drainage tunnel on both sides and toward the main powerhouse. Thus, the M41CF-01, M41CF-02, and M41CF-03 displacement meters started monitoring since the first layer of excavation in the main powerhouse in May 2018. Figure 5 shows the monitoring displacement variations obtained by these multi-point displacement meters, and the monitoring point near the wall of the main powerhouse is defined as the ostiole point for each multi-point displacement meter.

Figures 5a to 5c show that the displacement at the vault of the main powerhouse (monitored by the M41CF-01 displacement meter) has apparent changes in the first layer of excavation. The ostiole point on the M41CF-01 meter is near the wall of the main powerhouse, so it has the maximum displacement among the four monitoring points. After the first layer of excavation, the measured displacement of the ostiole point increases to 2.2 mm. Then, the measured displacement at the vault converges and has no noticeable change in the following excavations. The measured displacement at the upstream spandrel (monitored by the M41CF-02 displacement meter) increases to about 1 mm after the first layer of excavation. Then, the measured displacement of the upstream spandrel keeps a steady and slow growth trend, and it reaches the maximum displacement of about 2.5 mm after the fourth layer of excavation. The measured displacement at the downstream spandrel (monitored by the M41CF-03 displacement meter) increases in a staircase pattern during the initial two layers of excavation, and it stabilizes around 3.5 mm and 6 mm after the first and second layers of excavation, respectively. Then it has a steady and slow increasing trend during the third and fourth layers of excavation, and the maximum displacement at the downstream spandrel reaches about 10 mm.

The M41CF-04 and M61CF-05 multi-point displacement meters were installed after the third layer of excavation, and the M41CF-06 multi-point displacement meter

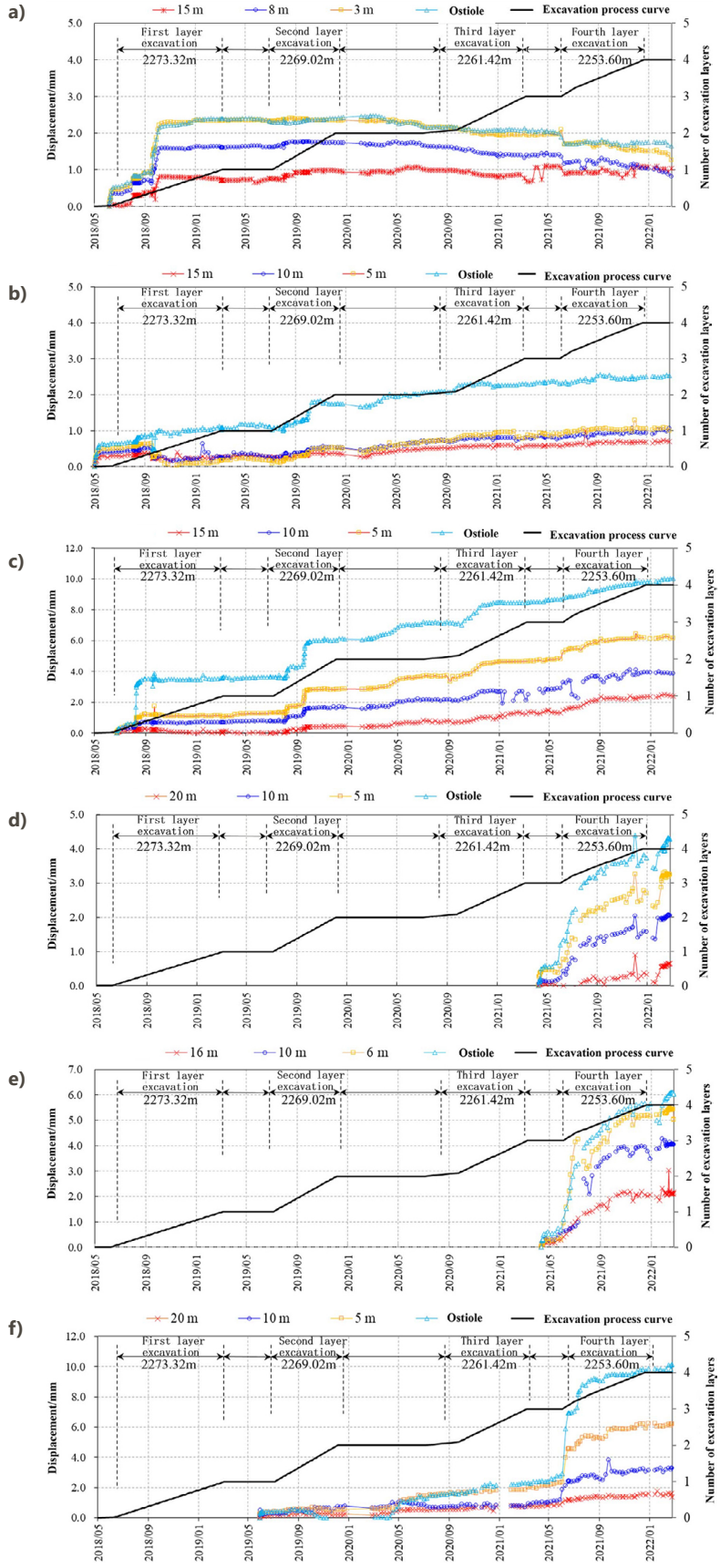

Figure 5. Monitoring displacements around the main powerhouse obtained by some multi-point displacement meters in the section of the 1# electric generator. Monitoring displacements of multi-point displacement meters: a – at the vault (M41CF-01); b – at the upstream spandrel (M41CF-02); c – at the downstream spandrel (M41CF-03); d – at the upstream rock anchor beam (M41CF-04); e – at the downstream rock anchor beam (M41CF-05); f – on the upstream sidewall (M41CF-06)

was installed from the upstream drainage tunnel after the first layer of excavation. Their measured displacement variations are shown in Figures 5d to 5f. The measured displacements at the upstream and downstream rock anchor beams (monitored by the M41CF-04 and M61CF-05 displacement meters) are significantly affected by the third and fourth layers of excavation, and both of them have a rising trend during the subsequent excavations. Thus, the deformations around the upstream and downstream rock anchor beams had not converged yet after the fourth layer of excavation. As of March 21, 2022, the maximum displacements measured by the M41CF-04 and M61CF-05 displacement meters are about 4.4 mm and 6.2 mm, respectively. Since the M41CF-06 displacement meter was installed before the main powerhouse was excavated to the elevation of its end, the initial three layers of excavation have relatively small influence on its deeply buried monitoring points, and its monitoring displacements are relatively small and show a slow increasing trend during these stages. The fourth layer of excavation makes surrounding rock near the end point of the M41CF-06 displacement meter exposed, so its monitoring displacement rises rapidly during this stage. After the fourth layer of excavation, the maximum monitoring displacement on the upstream sidewall is about 10.2 mm.

To analyze the overall response of the main powerhouse during the initial four layers of excavation, the maximum monitoring displacements measured by the multi-point displacement meters in the sections of 1# to 4# electric generators are presented in Figure 6 as of March 21, 2022.

Figure 6 shows that the surrounding rock deforms towards the cavern due to stress release during the initial four layers of excavation. The deformation response of surrounding rock differs at each location, but the overall deformation response of surrounding rock is small. The maximum displacement of entire surrounding rock is 10.2 mm and was measured on the upstream sidewall in the section of the 1# electric generator, and the maximum displacements of all the other positions are less than 10 mm. The deformations at the upstream spandrel and the vault of the main powerhouse are relatively small, and the deformations at the downstream spandrel and the downstream rock anchor beam are relatively large.

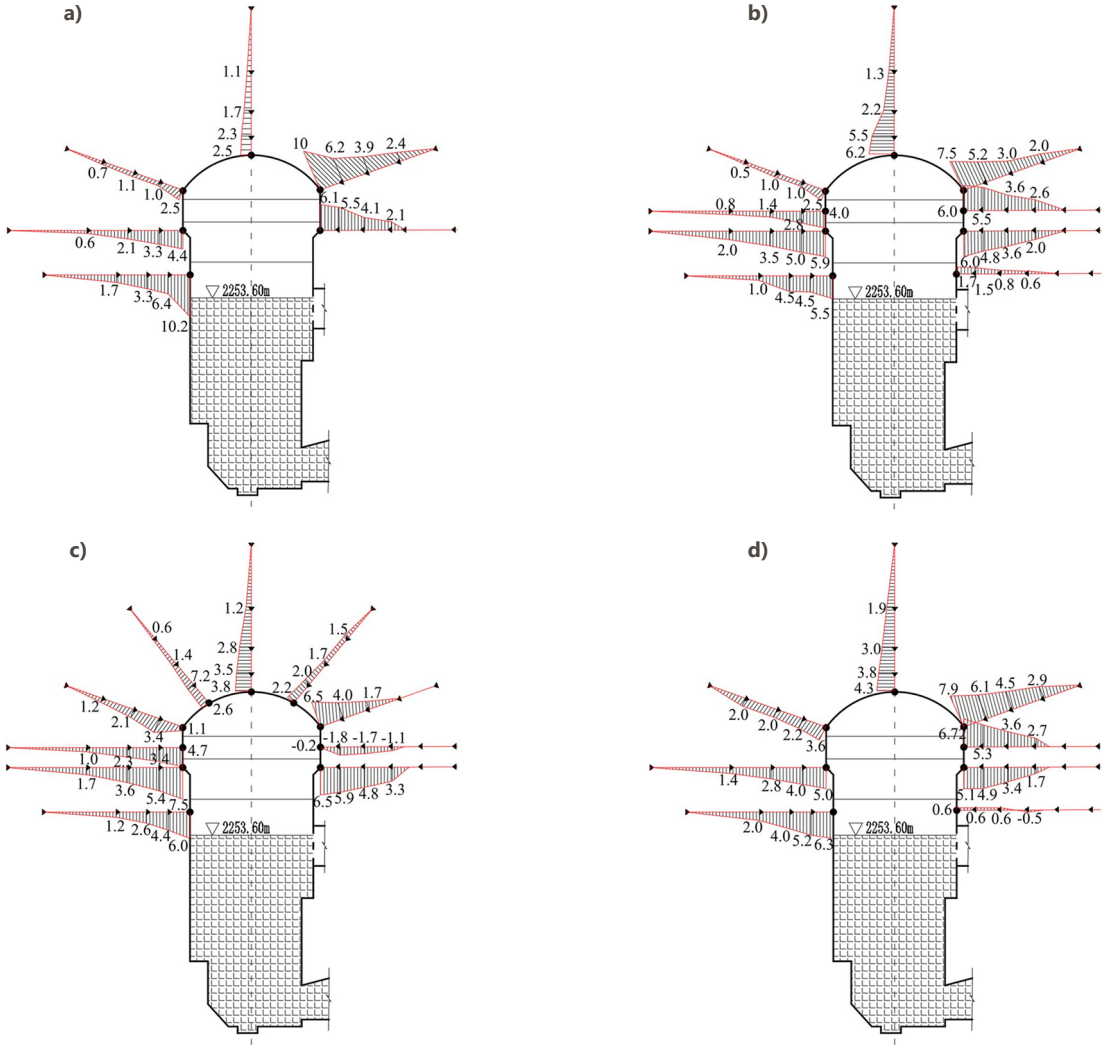

Figure 6. The maximum displacements measured by the multi-point displacement meters in the sections of a – 1#; b – 2#; c – 3#; d – 4# electric generators (unit: mm)

Besides, the deformation of surrounding rock gradually decreases, as the depth of surrounding rock increases. When the depth of surrounding rock exceeds 15 m, its displacement is less than 2 mm. The multi-point displacement meters on the downstream sidewall in the sections of 2# and 4# electric generators were installed at the end of December 2021, so their monitoring time is short and their monitoring displacements are small. Since the displacements of all the monitoring points are small, the surrounding rock of the main powerhouse is stable.

Table 2 shows the maximum monitoring displacements at various positions of the cavern's wall in all the monitoring sections of the main powerhouse. As shown in Table 2, the maximum deformations during the initial four layers of excavation that were obtained from different sections but at the same position are almost the same. The average deformation of surrounding rock at the upstream rock anchor beam is 4.3 mm, which is the smallest one around the cavern; and the average deformation of surrounding rock at the downstream spandrel is 8.7 mm, which is the largest one around the cavern. The main machine room, the installation room, and the auxiliary powerhouse have different shapes and geological conditions, so their deformations are also different. The deformations of surrounding rock in the main machine room are larger than the deformations of the other two rooms at the same position. In the four sections of the main machine room, the displacements of surrounding rock at the same position are almost equal, and their standard deviation is less than 2 mm. In the installation room, the maximum displacement of surrounding rock is 13.8 mm and occurs at the downstream spandrel. This is also the largest displacement among the monitoring displacements at the downstream spandrel because it is affected by the excavation of a traffic tunnel, which is located below the downstream spandrel. In the auxiliary powerhouse, the maximum displacement of surrounding rock is 14.7 mm and occurs at the vault. This deformation is the largest one among all the monitoring displacements and far more than the other monitoring displacements at the vault because the lamprophyre vein passes through the vault of the auxiliary powerhouse.

3.2. Analysis of monitoring data measured by bolt stress meters

Figure 7 presents the monitoring data of the bolt stress meters at different positions in all the monitoring sections.

Because some stress meters are broken or have a short monitoring time, only the monitoring data of the bolt stress meters at the vault, the upstream and downstream spandrels, and the upstream and downstream rock anchor beams are shown. Figure 7 shows that the monitoring data of the bolt stress meters vary significantly in magnitude. Because some of the bolt stress meters are close to blasting points, their monitoring stresses were dramatically influenced by the blast, and most of the impacts are irreversible. The bolt stress increased sharply in a short time during the blast, and the measured stress increased from a small value to more than 300 MPa. For example, the measured bolt stress at the upstream spandrel in the section of the 4# electric generator even reached 400 MPa, which has already exceeded the measuring range of the meter.

As shown in Figure 7a, the bolt stresses measured by most of the monitoring points at the vault are less than 100 MPa, except for the monitoring point at the vault of the auxiliary powerhouse. The measured bolt stresses keep constant after the first layer of excavation, so the subsequent excavations have little influence on the bolt stress at the vault. The variation trend of the bolt stress is the same as that of the monitoring displacement at the vault. However, the measured bolt stress at the vault of the auxiliary powerhouse increases to 300 MPa abruptly after a nearby blast during the first layer of excavation. As analyzed in the above section, the vault of the auxiliary powerhouse also experiences a large displacement of 14.7 mm due to the existence of the lamprophyre vein, so the deformation of the vein is sensitive to not only the stress distribution but also the blast. As shown in Figures 7b and 7c, the measured bolt stresses at the upstream and downstream spandrel are generally small. The measured bolt stresses at the spandrels increase slightly and then tend to be stable during the second layer of excavation, and the subsequent excavations have little influence on it. Due to

Table 2. The maximum displacements on the cavern's wall in all the sections (unit: mm)

Position	The maximum displacements on the cavern's wall						Average displacement	Standard deviation	
	1-1	2-2	3-3	4-4	5-5	6-6		1~4 sections	All sections
Vault	2.5	6.2	3.8	4.3	2.4	14.7	5.7	1.3	4.2
Upstream spandrel	2.5	2.5	3.4	3.6	6.7	8.8	4.6	0.5	2.4
Downstream spandrel	10.0	7.5	6.5	7.9	13.8	6.3	8.7	1.3	2.6
Upstream rock anchor beam	4.4	4.0	4.7	5.0	3.5	–	4.3	0.4	0.5
Downstream rock anchor beam	6.1	6.0	6.5	5.1	–	7.4	6.2	0.5	0.7
Upstream sidewall	10.2	5.5	6.0	6.3	–	6.5	6.9	1.9	1.7

Note: "–" indicates the multi-point displacement meter at this position is broken.

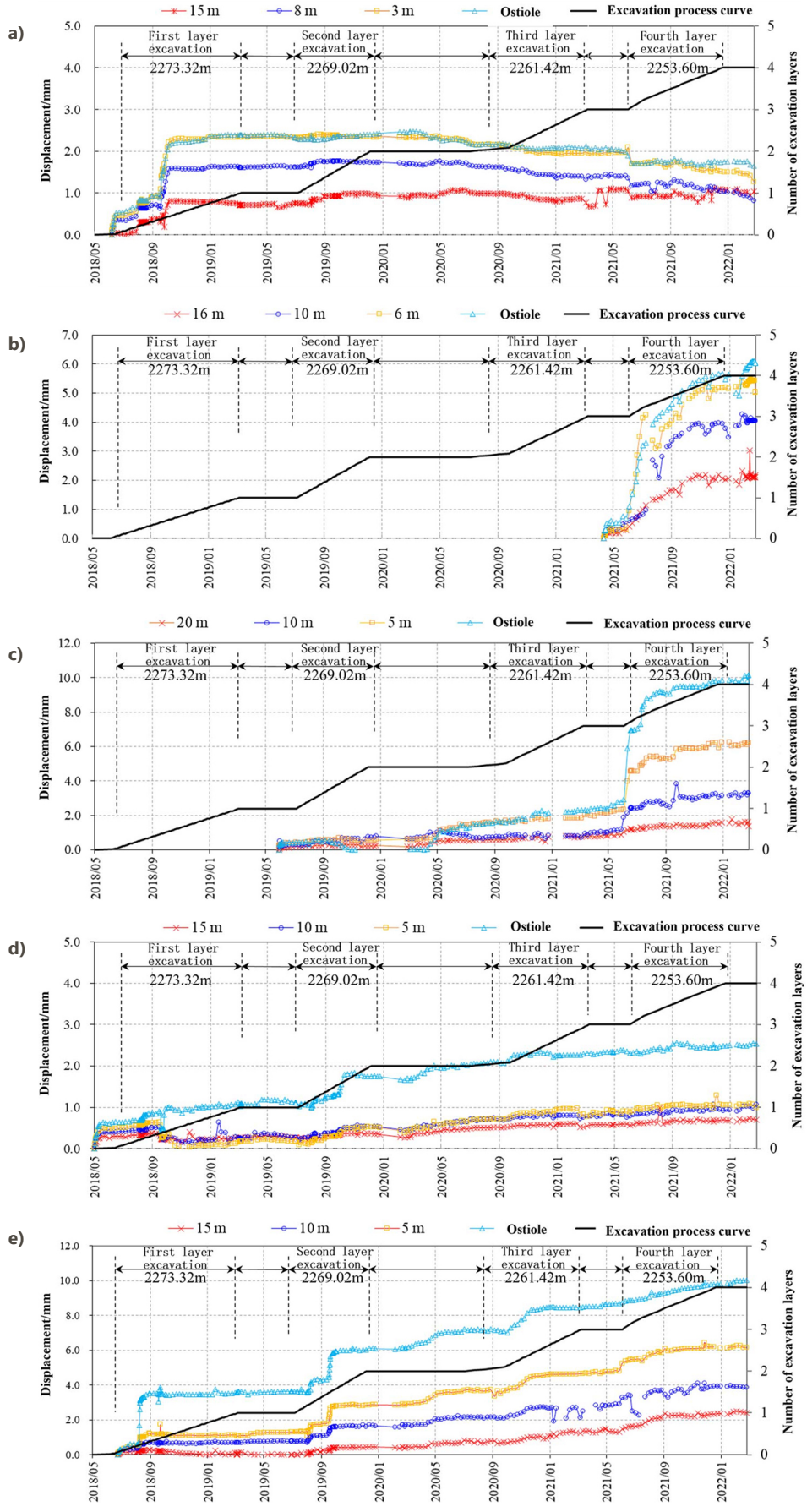

Figure 7. Stress monitoring curve of bolt stress meters in the powerhouse at: a – the vault; b – the upstream spandrel; c – the downstream spandrel; d – the upstream side wall; e – the downstream side wall

nearby blasts, the measured bolt stresses at the upstream spandrel in the section of the 4# electric generator and the downstream spandrel in the section of the 3# electric generator increase abruptly and reach 400 MPa and 380 MPa, respectively. As shown in Figures 7d and 7e, the monitoring time of the bolt stress meters around the upstream and downstream rock anchor beam are relatively short as of March 2022. Some anchors are pre-tensioned by 150 kN after installation, so these anchors have relatively high stresses at the beginning. Then, their stresses tend to increase slowly during the third and fourth layers of excavation.

As shown by the monitoring data of the bolt stress meter at the vault in Figure 7a, the monitoring stress at the vault of the auxiliary powerhouse did not change when the excavation was stopped. Thus, the deformation of the lamprophyre vein is mainly affected by the stress adjustment of surrounding rock caused by excavation, and it did not present significant deformation or slippage trend during the downtime, which means that it is in a stable state.

4. Numerical simulation

The excavation of the Shuangjiangkou underground powerhouse is ongoing, so it is important to scientifically analyze and predict the response characteristics of surrounding rock during the subsequent excavations of the powerhouse, especially, to investigate the influence of the lamprophyre vein on the subsequent excavations. In the following analysis, the mechanical parameters of surrounding rock were inversely analyzed based on the existing monitoring data and then brought into a finite difference numerical model in FLAC3D to simulate the subsequent excavations.

4.1. Back analysis of surrounding rock parameters

In order to improve the accuracy of numerical simulation in rock engineering, intelligent algorithms have been widely applied to the stability analysis of surrounding rock (Khayrutdinov et al., 2022; Lawal & Kwon, 2021). The particle swarm optimization back propagation (PSO-BP) neural network algorithm was used to inversely analyze the mechanical parameters of surrounding rock. The F1 fault crosses the main powerhouse around the 3# electric generator, so the section of the 3# electric generator was chosen as the characteristic section to conduct the back analysis. The measured displacement increments of the monitoring points in the section of the 3# electric generator during the fourth layer of excavation were taken as the input values of back analysis, as listed in Table 3.

There are six input values, so the node number in the input layer of the neural network is 6. The mechanical behavior of surrounding rock was assumed to follow the Mohr-Coulomb criterion, which has four mechanical parameters, i.e., elastic modulus, Poisson's ratio, friction angle, and cohesion, so the node number in the output layer of the neural network is 4. Besides, the neural network was set to have two hidden layers, which contain 13 and 4 nodes, respectively. Thus, a 6-13-4-4 topology network was constructed for the back analysis. Before conducting the back analysis, numerical simulations were carried out to obtain the training samples of the neural network. The initial training sample was calculated by floating the constitutive parameters suggested in the geological survey report up and down by 10%, 20%, and 30%, respectively. Since there were 4 parameters and each parameter had 7 levels, an orthogonal test scheme L49(7^4) was designed, as listed in Table 4. 49 groups of mechanical parameters generated by the orthogonal test scheme were substituted into the numerical model for excavation simulation, and the numerical simulations resulted in 49 groups of displacement increments. By setting the simulated displacement and these four mechanical parameters as the inputs and outputs of the neural network, the neural network is trained to effectively reflect the nonlinear relationship between displacements and parameters of surrounding rock. Then, the displacement increments listed in Table 3 were substituted into the trained neural network to obtain the mechanical parameters of the onsite surrounding rock. The suggested surrounding rock parameters in the geological survey report and back-analyzed values are listed in Table 5. These back-analyzed parameters were used to predict the displacement responses, stress responses, and the stability of surrounding rock during the subsequent excavations.

Table 3. Measured displacement increments of the monitoring points in the section of the 3# electric generator during the fourth layer of excavation

No.	Position	Displacement increments (mm)
M43-01	Vault	0.33
M43-04	Upstream spandrel	1.57
M43-05	Downstream spandrel	1.96
M43-08	Upstream rock anchor beam	4.53
M63-09	Downstream rock anchor beam	5.61
M43-10	Upstream sidewall	5.83

4.2. Numerical model

The numerical model mainly includes the mountain, main powerhouse, auxiliary powerhouse, installation room, main transformer chamber, tailrace surge chamber, omnibus bar cave, tailrace tunnel, and other chambers. The support structure considered in the simulation includes ordinary mortar bolts, pre-tensioned bolts, and pre-tensioned anchor cables in three large chambers. The lamprophyre vein and the F1 fault are also considered in the simulation to analyze their influences on the deformation and stress of surrounding rock. The model is shown in Figure 8. In the simulation, the normal displacement constraints were applied on the front, back, left, right and bottom sides of the model. Based on the in-situ stress measurement results

Table 4. L49(7^4) orthogonal test scheme

No.	Elastic modulus E (GPa)	Poisson's ratio v	Friction angle ϕ (°)	Cohesion c (MPa)	No.	Elastic modulus E (GPa)	Poisson's ratio v	Friction angle ϕ (°)	Cohesion c (MPa)
1	24.50	0.18	35.70	0.91	26	24.50	0.20	45.90	1.04
2	38.50	0.30	66.30	1.04	27	38.50	0.33	40.80	1.17
3	28.00	0.25	61.20	1.17	28	28.00	0.28	35.70	1.30
4	42.00	0.20	56.10	1.30	29	31.50	0.30	40.80	1.30
5	31.50	0.33	51.00	1.43	30	45.50	0.25	35.70	1.43
6	45.50	0.28	45.90	1.56	31	35.00	0.20	66.30	1.56
7	35.00	0.23	40.80	1.69	32	24.50	0.33	61.20	1.69
8	38.50	0.25	45.90	1.69	33	38.50	0.28	56.10	0.91
9	28.00	0.20	40.80	0.91	34	28.00	0.23	51.00	1.04
10	42.00	0.33	35.70	1.04	35	42.00	0.18	45.90	1.17
11	31.50	0.28	66.30	1.17	36	45.50	0.20	51.00	1.17
12	45.50	0.23	61.20	1.30	37	35.00	0.33	45.90	1.30
13	35.00	0.18	56.10	1.43	38	24.50	0.28	40.80	1.43
14	24.50	0.30	51.00	1.56	39	38.50	0.23	35.70	1.56
15	28.00	0.33	56.10	1.56	40	28.00	0.18	66.30	1.69
16	42.00	0.28	51.00	1.69	41	42.00	0.30	61.20	0.91
17	31.50	0.23	45.90	0.91	42	31.50	0.25	56.10	1.04
18	45.50	0.18	40.80	1.04	43	35.00	0.28	61.20	1.04
19	35.00	0.30	35.70	1.17	44	24.50	0.23	56.10	1.17
20	24.50	0.25	66.30	1.30	45	38.50	0.18	51.00	1.30
21	38.50	0.20	61.20	1.43	46	28.00	0.30	45.90	1.43
22	42.00	0.23	66.30	1.43	47	42.00	0.25	40.80	1.56
23	31.50	0.18	61.20	1.56	48	31.50	0.20	35.70	1.69
24	45.50	0.30	56.10	1.69	49	45.50	0.33	66.30	0.91
25	35.00	0.25	51.00	0.91					

Table 5. The suggested parameters in the geological survey report and back-analyzed mechanical parameters of surrounding rock

Type	Elastic modulus E (GPa)	Poisson's ratio v	Friction angle ϕ (°)	Cohesion c (MPa)
Suggested parameters	32.9	0.25	52.4	1.50
Back-analyzed parameters	36.4	0.26	58.2	1.48

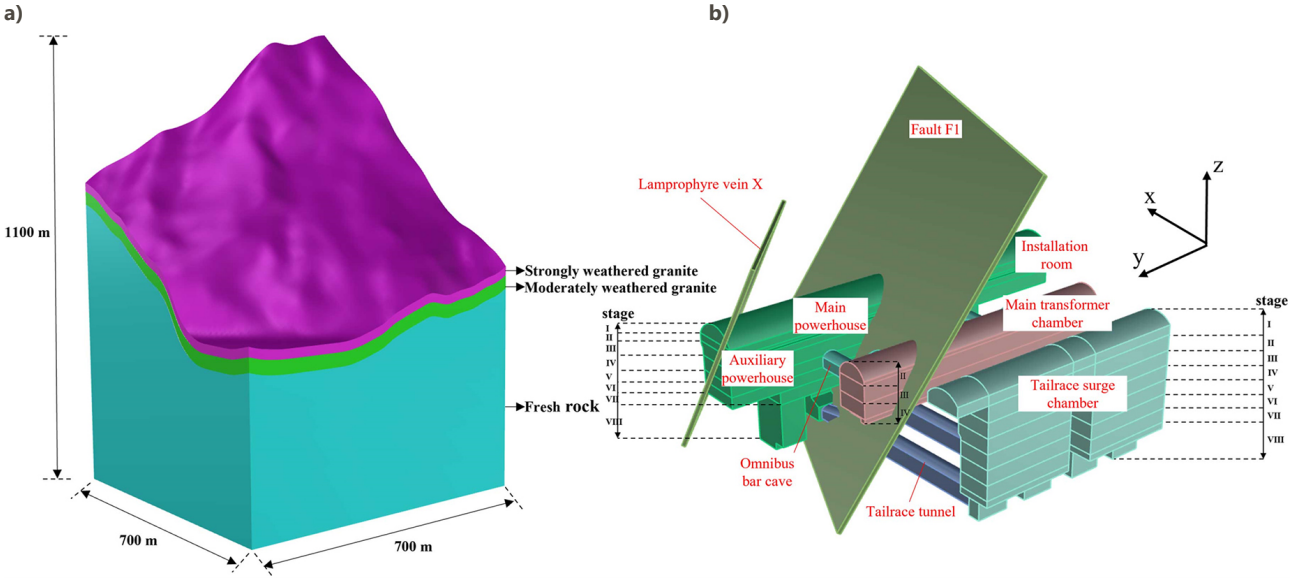

Figure 8. The numerical model consists of: a – the mountain and b – the underground caverns and main geological structures

around the Shuangjiangkou underground powerhouse, the initial in-situ stress field and boundary conditions for modelling the stress state of rock masses have been inversely analyzed by the authors' coworkers (Yan et al., 2023), so their analysis results of the in-situ stress were served as boundary conditions for the numerical model.

4.3. Prediction of surrounding rock's displacement

Figure 9 shows the simulated displacement distributions of surrounding rock in the section of the 3# electric generator of the main powerhouse after all the excavation. In the section of the 3# electric generator, the maximum horizontal deformation is 31.8 mm and occurs at the upstream sidewall of the main powerhouse, and the maximum horizontal deformation of the downstream sidewall is 26.5 mm. The surrounding rock at the vault of the main powerhouse deforms towards the cavern and its vertical deformation is relatively small after excavation. Besides, the F1 fault passes through the surrounding rock above the main transformer chamber, so the vertical deformation around its arch is relatively large and has a maximum value of 14.1 mm. The maximum vertical deformation on the floor of the main transformer chamber is 18.4 mm.

Figure 10 shows the simulated displacement distributions of surrounding rock in the longitudinal section of the main powerhouse after all the excavation. In the longitudinal section of the main powerhouse, the end wall of the main powerhouse deforms towards the cavern. Because the lamprophyre vein intersects with the end wall of the auxiliary powerhouse, the simulated deformation on the end wall of the auxiliary powerhouse is much more significant. After all the excavation of the powerhouse, the maximum horizontal displacement of surrounding rock on the end wall of the auxiliary powerhouse is 29.6 mm. The horizontal deformation on the end wall of the installation room is relatively small, and its maximum horizontal displacement is 16.4 mm. Besides, the F1 fault passes through the main powerhouse, and the surrounding rock on both sides of the fault shows the characteristic of shear-dislocation deformation. The maximum vertical deformation of surrounding rock at the vault is 25.0 mm and occurs in the section between the 2# and 3# electric generator, and the maximum vertical deformation on the floor is 33.1 mm.

4.4. Prediction of surrounding rock's stress

Figure 11 shows the simulated principal stress distributions of surrounding rock in the section of the 3# electric generator of the main powerhouse. After the excavation of the main powerhouse, the radial stresses around these caverns are released by the excavation. The first principal stress of surrounding rock within 8 m depth of the upstream and downstream sidewalls decreases to less than 10 MPa, and the third principal stress of surrounding rock within 15m depth of the sidewalls decreases to less than 4 MPa. The circumferential stress concentrates around these caverns, especially in the omnibus bar cave and the tailrace tunnel.

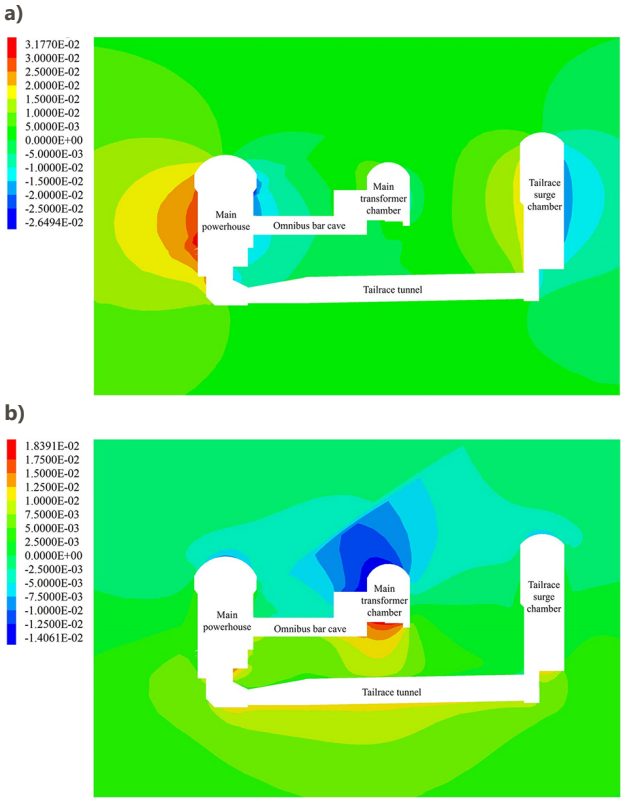

Figure 9. Simulated displacement distributions of surrounding rock in the section of the 3# electric generator of the main powerhouse after all the excavation. The displacement distributions in the a – X and b – Z direction (unit: m)

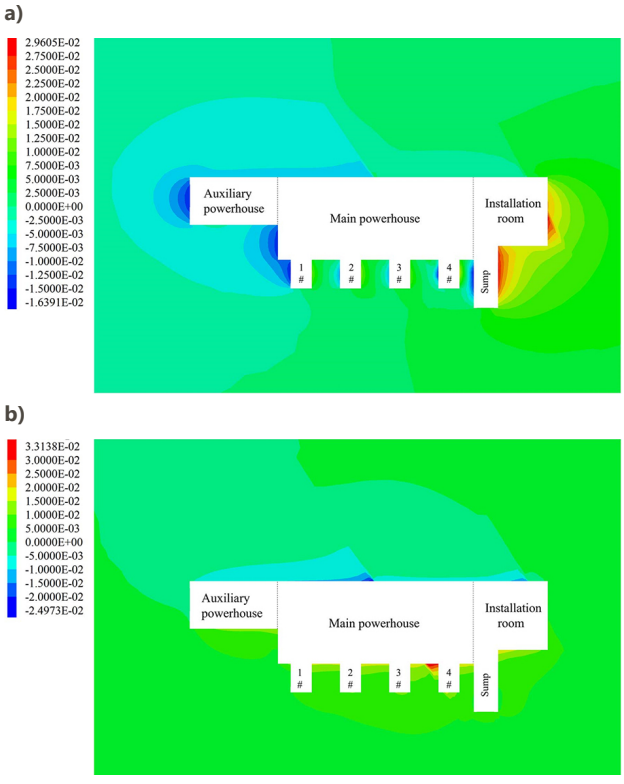

Figure 10. Simulated displacement distributions of surrounding rock in the longitudinal section of the main powerhouse after all the excavation. The displacement distributions in the a – Y and b – Z direction (unit: m)

The first principal stress at the vault of the tailrace tunnel is significantly larger than that of other positions, and the maximum first principal stress is 44.5 MPa. Thus, attention should be paid to the vault of the omnibus bar cave and the tailrace tunnel during the subsequent excavations. Tensile stress appears in some surrounding rocks of the main powerhouse, but its values are less than 0.22 MPa, which could not cause tensile fractures.

Figure 12 shows the simulated principal stress distributions of surrounding rock in the longitudinal section of the main powerhouse. After the excavation of the main powerhouse, the stress concentrates in some small areas in the longitudinal section of the main powerhouse. The stress mainly concentrates at the top of the end wall in the auxiliary powerhouse, the bottom corner of the end wall in the installation room, and the connection part of the tailrace tunnel. The maximum first principal stress is 37.2 MPa. However, the third principal stress around the main powerhouse decreases significantly in a large range of surrounding rocks. Affected by the lamprophyre vein, stress concentrates on the end wall of the auxiliary powerhouse. The influence of the F1 fault on the stress around the main powerhouse is not apparent, as indicated by the contour.

4.5. Prediction of bolt's displacement and stress

The simulated displacement distributions of bolts around the main powerhouse are shown in Figure 13. After all the excavation of the main powerhouse, the displacements of bolts are relatively large. Because the lamprophyre vein and F1 fault intersect with the main powerhouse, the maximum displacement of the bolt around these two unfavorable geological structures is 36.7 mm. The displacements of the other bolts in the surrounding rock are generally less than 2 mm, so the last four layers of excavation of the main powerhouse have relatively small influence on their displacements. Figure 14 shows the simulated axial stress distributions of bolts around the main powerhouse. After the excavation of the main powerhouse, the stresses of most of the bolts are tensile stress, but the stresses of some bolts are compressive stress. The tensile stresses are generally larger than 100 MPa. The tensile stresses of some bolts in the auxiliary powerhouse and the main transformer chamber exceed the bolt's strength (400 MPa) because these bolts penetrate the lamprophyre vein and the F1 fault. The engineering treatment should be intensified for the lamprophyre vein and the F1 fault.

5. Discussion

The on-site construction of underground caverns is a step-by-step process, and the deformation and failure of surrounding rock are affected by various factors. Many studies have used numerical methods to verify or predict the stability of underground caverns (Sari, 2022; Vo et al., 2022). However, since the mechanical parameters of the surrounding rock used in numerical simulations are often

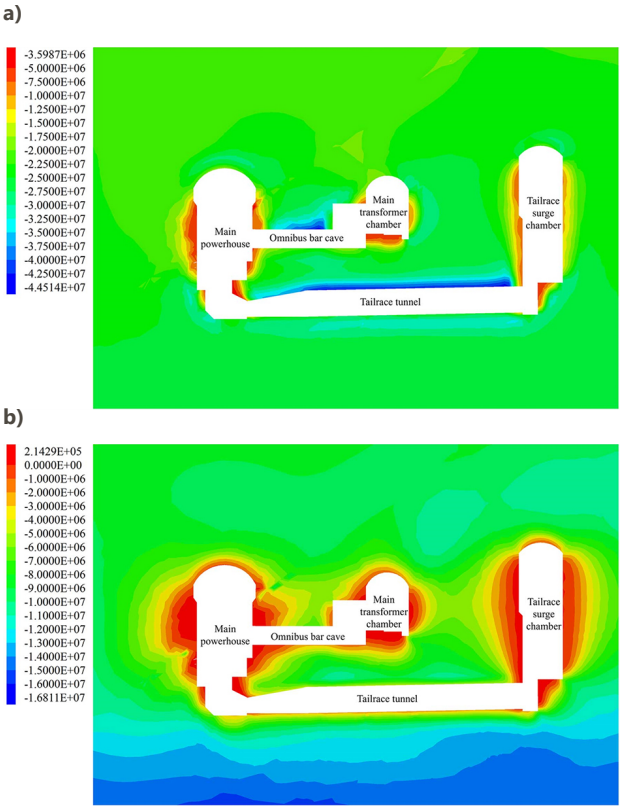

Figure 11. Simulated principal stress distributions of surrounding rock in the section of the 3# electric generator of the main powerhouse after all the excavation. a – The first and b – the third principal stresses (unit: Pa)

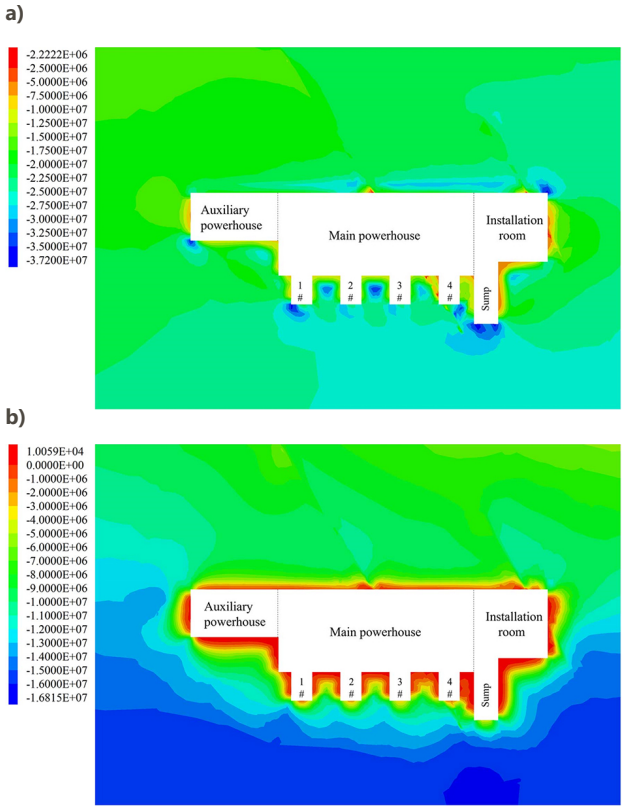

Figure 12. Simulated principal stress distributions of surrounding rock in the longitudinal section of the main powerhouse after all the excavation. a – The first and b – the third principal stresses (unit: Pa)

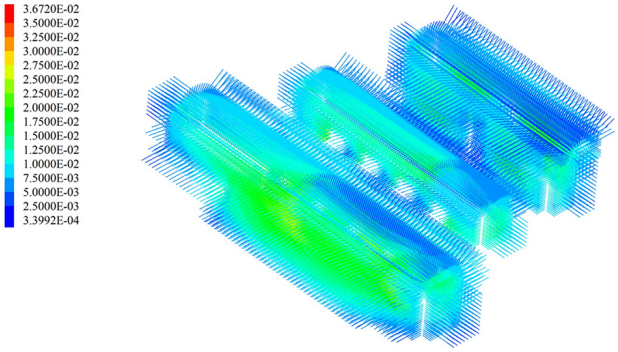

Figure 13. Simulated displacement distributions of bolts around the main powerhouse after all the excavation (unit: m)

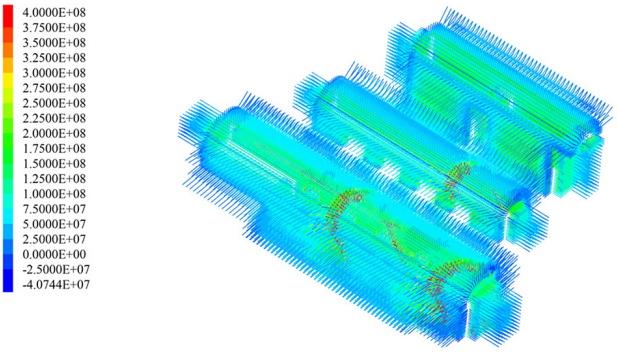

Figure 14. Simulated axial stress distributions of bolts around the main powerhouse after all the excavation (unit: Pa)

empirical or measured in the laboratory and differ from the actual situation in the field, it will inevitably lead to a certain degree of inaccuracy. In our research, the mechanical parameters of the surrounding rock were inversely analyzed by the PSO-BP algorithm. The accuracy of the PSO-BP algorithm has been validated by the authors' coworkers (Yan et al., 2023), so the mechanical parameters and stress boundary conditions obtained by back analysis could reflect the properties and stress conditions of surrounding rock very well, and they can ensure the reliability of the numerical results. Furthermore, many scholars have proposed various methods for analyzing the stability of underground caverns, such as an early warning method for potential damage in deep buried tunnels based on multi-source monitoring (Sun et al., 2021), a stability evaluation method for underground caverns combining microseismic monitoring and numerical simulation (Ma et al., 2016). The above methods have their own unique aspects and advantages. However, when they are compared to the method that combines conventional monitoring, back analysis, and numerical simulation as shown in our analysis, our method is more applicable and economical.

In this study, the prediction was made based on the monitoring data obtained after the first four layers of excavation. The accuracy of the prediction needs time to verify and could only be verified after the entire excavations of the underground powerhouse, because the mechanical parameters of surrounding rock inversely analyzed from the first four layers of excavations may not well represent the properties of rock mass surrounding the completely excavated cavern. Besides, the stability prediction was made on the overall stability analysis of surrounding rock, but there is a lack of analysis on the local stability of surrounding rock, such as the stability of rock blocks. Therefore, further research can be conducted on the local stability of surrounding rock under the influence of multiple factors. In addition, cause analysis of some abnormal monitoring data and correlation analysis between two types of monitoring data are still not enough. Due to the huge monitoring data of underground powerhouses, more computer technologies, such as big data mining analysis, can be used to analyze these huge monitoring data.

6. Conclusions

As of March 2022, the initial four layers of the Shuangjiangkou underground powerhouse have been excavated, and the monitoring data measured by multi-point displacement meters and bolt stress meters were investigated to reveal the main influence factors on the stability of surrounding rock masses. Then, they were used to inversely analyze the mechanical parameters of surrounding rock masses, and the stability of surrounding rock masses during the subsequent excavations was studied by numerical simulation. The following conclusions were drawn:

1) After analyzing the monitoring data collected on-site, it was determined that the overall deformation of surrounding rock during the initial four layers of excavation was relatively small, and the surrounding rock deformed to the interior of the cavern due to stress release. The surrounding rock are generally stable. However, due to the influence of the lamprophyre vein, the F1 fault and the excavation blast, there are some local failures in the surrounding rock.

2) Based on the monitoring data in the section of the 3# electric generator during the fourth layer of excavation, the mechanical parameters of the surrounding rock were inversely analyzed. The elastic modulus and friction angle obtained from the inversion are 3.5 GPa and 5.8 degrees larger than the suggested values in the geological survey report, respectively. The simulated displacement increments of the monitoring points after back analysis are closer to the measured increments, so the feasibility and practicability of the entire back analysis process are demonstrated.

3) The numerical simulation results provide a basis for evaluating the stability of surrounding rock during the subsequent excavations of the underground powerhouse. The numerical analysis shows that the omnibus bar cave and the tailrace tunnel are at the greatest risk of instability. Therefore, the monitoring and engineering treatment of the surrounding rock in the omnibus bar cave and the tailrace tunnel should be strengthened.

Acknowledgements

The authors would like to thank Dr. Huai-Zhong Liu and Dr. Hong-Chuan Yan from the College of Water Resource and Hydropower of Sichuan University for their contributions to the numerical analysis.

Funding

This work was supported by the <The National Natural Science Foundation of China #1> under Grant [number 52104143]; <The Natural Science Foundation of Sichuan Province, China #2> under Grant [number 2022NSFSC0193].

Author contributions

Jiang-Da He conceived the study and developed the overarching research goals. You Li wrote the first draft of the article. Ming-Li Xiao and Gan Feng edited the draft of the manuscript. Ming-Guang Cai and Jian-Liang Pei were responsible for data collection and analysis. Jia-Ming Wu carried out the numerical simulation.

Disclosure statement

The Authors declare this paper does not have any competing financial, professional, or personal interests from other parties.

References

Bacova, D., Khairutdinov, A. M., & Gago, F. (2021). Cosmic geodesy contribution to geodynamics monitoring. *IOP Conference Series: Earth and Environmental Science*, *906*, Article 012074. https://doi.org/10.1088/1755-1315/906/1/012074

Blake, W. (1974). *Microseismic techniques for monitoring the behavior of rock structures* (Vol. 665). US Department of the Interior, Bureau of Mines.

Chandra, S., Nilsen, B., & Lu, M. (2010). Predicting excavation methods and rock support: a case study from the Himalayan region of India. *Bulletin of Engineering Geology and the Environment*, *69*, 257–266. https://doi.org/10.1007/s10064-009-0252-8

Choi, S. W., Lee, J., Oh, B. K., & Park, H. S. (2016). Analytical models for estimation of the maximum strain of beam structures based on optical fiber Bragg grating sensors. *Journal of Civil Engineering and Management*, *22*(1), 86–91. https://doi.org/10.3846/13923730.2014.897976

Dhawan, K., Singh, D., & Gupta, I. D. (2004). Three-dimensional finite element analysis of underground caverns. *International Journal of Geomechanics*, *4*(3), 224–228. https://doi.org/10.1061/(ASCE)1532-3641(2004)4:3(224)

Ding, X., & Qin, H. (2000). Geotechnical instruments in structural monitoring. *Journal of Geospatial Engineering*, *2*(1), 45–56.

Gholizadeh, S., Leman, Z., & Baharudin, B. T. H. T. (2015). A review of the application of acoustic emission technique in engineering. *Structural Engineering and Mechanics*, *54*(6), 1075–1095. https://doi.org/10.12989/sem.2015.54.6.1075

Gong, H., Kizil, M. S., Chen, Z., Amanzadeh, M., Yang, B., & Aminossadati, M. S. (2019). Advances in fibre optic based geotechnical monitoring systems for underground excavations. *International Journal of Mining Science and Technology*, *29*(2), 229–238. https://doi.org/10.1016/j.ijmst.2018.06.007

Hanna, T. H. (1985). *Field instrumentation in geotechnical engineering*. Trans Tech Publications.

He, J., Li, X., Deng, X., Zhang, S., & Qin, L. (2021). Mechanical properties and stability analysis of surrounding rock of underground cavern under various stress loading paths. *IOP Conference Series: Earth and Environmental Science*, *861*, Article 042012. https://doi.org/10.1088/1755-1315/861/4/042012

Khayrutdinov, M., Kongar-Syuryun, C. B., Khayrutdinov, A. M., & Tyulyaeva, Y. S. (2021). Improving safety when extracting water-soluble ores by optimizing the parameters of the backfill mass. *Monthly Journal of Research and Production*, *2021*, 53–59. https://doi.org/10.24000/0409-2961-2021-1-53-59

Khayrutdinov, M. M., Golik, V. I., Aleksakhin, A. V., Trushina, E. V., Lazareva, N. V., & Aleksakhina, Y. V. (2022). Proposal of an algorithm for choice of a development system for operational and environmental safety in mining. *Resources*, *11*(10), Article 88. https://doi.org/10.3390/resources11100088

Kuili, S., & Sastry, V. R. (2023). A numerical modelling mpproach to mssess deformations of horseshoe cavern on account of rock mass characteristics and discontinuities. *International Journal of Engineering*, *36*(7), 1259–1268. https://doi.org/10.5829/IJE.2023.36.07A.07

Kumar, V., Jha, P. C., Singh, N. P., & Cherukuri, S. (2021). Dynamic stability evaluation of underground powerhouse cavern using microseismic monitoring. *Geotechnical and Geological Engineering*, *39*(3), 1795–1815. https://doi.org/10.1007/s10706-020-01588-9

Lanciano, C., Vanneschi, C., Tufarolo, E., & Salvini, R. (2021). Distributed optical fiber sensors and terrestrial laser scanner surveys for the monitoring of an underground marble quarry. *Italian Journal of Engineering Geology and Environment*, *2021*, 117–125. https://doi.org/10.4408/IJEGE.2021-01.S-11

Lawal, A. I., & Kwon, S. (2021). Application of artificial intelligence to rock mechanics: An overview. *Journal of Rock Mechanics and Geotechnical Engineering*, *13*(1), 248–266. https://doi.org/10.1016/j.jrmge.2020.05.010

Lechner, W., & Baumann, S. (2000). Global navigation satellite systems. *Computers and Electronics in Agriculture*, *25*(1–2), 67–85. https://doi.org/10.1016/S0168-1699(99)00056-3

Li, Y., Chen, Y., Jiang, Q., Hu, R., & Zhou, C. (2014). Performance assessment and optimization of seepage control system: a numerical case study for Kala underground powerhouse. *Computers and Geotechnics*, *55*, 306–315. https://doi.org/10.1016/j.compgeo.2013.09.013

Ma, K., Tang, C. A., Wang, L. X., Tang, D. H., Zhuang, D. Y., Zhang, Q. B., & Zhao, J. (2016). Stability analysis of underground oil storage caverns by an integrated numerical and microseismic monitoring approach. *Tunnelling and Underground Space Technology*, *54*, 81–91. https://doi.org/10.1016/j.tust.2016.01.024

Ma, K., Tang, C. A., Liang, Z. Z., Zhuang, D. Y., & Zhang, Q. B. (2017). Stability analysis and reinforcement evaluation of high-steep rock slope by microseismic monitoring. *Engineering Geology*, *218*, 22–38. https://doi.org/10.1016/j.enggeo.2016.12.020

Ma, K., Feng, B., Zhuang, D. Y., Guo, X. F., & Gao, Q. (2020a). Distance effects of the fault on the surrounding rock mass stability of the main powerhouse at the Huanggou pumped-storage power station. *Tunnelling and Underground Space Technology*, *106*, Article 103568. https://doi.org/10.1016/j.tust.2020.103568

Ma, K., Zhang, J., Zhou, Z., & Xu, N. (2020b). Comprehensive analysis of the surrounding rock mass stability in the underground

caverns of Jinping I hydropower station in Southwest China. *Tunnelling and Underground Space Technology*, *104*, Article 103525. https://doi.org/10.1016/j.tust.2020.103525

Ma, H.-P., Daud, N. N. N., Yousof, Z. M., Yaacob, W. Z., & He, H.-J. (2023). Stability analysis of surrounding rock of an underground cavern group and excavation scheme optimization: Based on an optimized DDARF method. *Applied Sciences*, *13*(4), Article 2152. https://doi.org/10.3390/app13042152

Małkowski, P., Niedbalski, Z., & Bednarek, L. (2021). Automatic monitoring system designed for controlling the stability of underground excavation. *Journal of the Polish Mineral Engineering Society*, *2*(1), 15–30. http://doi.org/10.29227/IM-2021-02-01

Manthei, G., & Plenkers, K. (2018). Review on in situ acoustic emission monitoring in the context of structural health monitoring in mines. *Applied Sciences*, *8*(9), Article1595. https://doi.org/10.3390/app8091595

Menéndez, J., Schmidt, F., Konietzky, H., Sánchez, A. B., & Loredo, J. (2020). Empirical analysis and geomechanical modelling of an underground water reservoir for hydroelectric power plants. *Applied Sciences*, *10*(17), Article 5853. https://doi.org/10.3390/app10175853

Mikolas, M., Mikusinec, J., Abrahamovsky, J., Dibdiakova, J., Tyulyaeva, Y., & Srek, J. (2021). Activities of a mine surveyor and a geologist at design bases in a limestone quarry. *IOP Conference Series: Earth and Environmental Science*, *906*, Article 012073. https://doi.org/10.1088/1755-1315/906/1/012073

Moomivand, H., Moosazadeh, S., & Gilani, S.-O. (2022). A new empirical approach to estimate the ratio of horizontal to vertical in-situ stress and evaluation of its effect on the stability analysis of underground spaces. *Rudarsko-geološko-naftni zbornik*, *38*(3), 97–107. https://doi.org/10.17794/rgn.2022.3.8

Ono, K. (2018). Review on structural health evaluation with acoustic emission. *Applied Sciences*, *8*(6), Article 958. https://doi.org/10.3390/app8060958

Prajapati, S. K., & Verma, A. (2023). Effect of fault characteristics on plastic zones around parallelly spaced two underground caverns and shear displacement along the fault plane. *Journal of the Geological Society of India*, *99*(6), 765–772. https://doi.org/10.1007/s12594-023-2383-0

Qian, Q., & Zhou, X. (2018). Failure behaviors and rock deformation during excavation of underground cavern group for Jinping I hydropower station. *Rock Mechanics and Rock Engineering*, *51*, 2639–2651. https://doi.org/10.1007/s00603-018-1518-x

Rahimi, B., Sharifzadeh, M., Feng, X.-T. (2021). A comprehensive underground excavation design (CUED) methodology for geotechnical engineering design of deep underground mining and tunneling. *International Journal of Rock Mechanics and Mining Sciences*, *143*, Article 104684. https://doi.org/10.1016/j.ijrmms.2021.104684

Rajabi, M., Rahmannejad, R., & Rezaei, M. (2021). Studying the deformation and stability of rock mass surrounding the power station caverns using NA and GEP models. *Structural Engineering and Mechanics*, *79*, 35–50.

Rezaei, M., & Rajabi, M. (2018). Vertical displacement estimation in roof and floor of an underground powerhouse cavern. *Engineering Failure Analysis*, *90*, 290–309. https://doi.org/10.1016/j.engfailanal.2018.03.010

Sainoki, A., Maina, D., Schwartzkopff, A. K., Obara, Y., & Karakus, M. (2020). Impact of the intermediate stress component in a plastic potential function on rock mass stability around a sequentially excavated large underground cavity. *International Journal of Rock Mechanics and Mining Sciences*, *127*, 104223. https://doi.org/10.1016/j.ijrmms.2020.104223

Sari, M. (2022). Two-and three-dimensional stability analysis of underground storage caverns in soft rock (Cappadocia, Turkey) by finite element method. *Journal of Mountain Science*, *19*(4), 1182–1202. https://doi.org/10.1007/s11629-021-7047-1

Sudhakar, K., Sinha, R. K., & Naik, S. R. (2023). Study on the impact of different parameters on prediction of crown deformations in underground caverns. *Sustainability*, *15*(17), Article 12851. https://doi.org/10.3390/su151712851

Sun, X., Zhu, J., Xu, Y., Ren, C., Yang, K., Zhang, F., Zhao, W., & Yuan, J. (2021). Multisource monitoring and early warning system of rock burst in the Gaoloushan deep-buried tunnel. *IOP Conference Series: Earth and Environmental Science*, *861*, Article 042028. https://doi.org/10.1088/1755-1315/861/4/042028

Sun, Y., Mao, H., Dong, L., Li, B., & Xu, N. (2023). Stability analysis of surrounding rock mass in underground caverns considering damage effect of microfractures. In *Rock Dynamics: Progress and Prospect, Proceedings of the Fourth International Conference on Rock Dynamics And Applications* (Vol. 1). CRC Press. https://doi.org/10.1201/9781003359142-36

Vo, T., Dang, V., Do, A. N., & Do, T. N. (2022). Study on the stability of rock mass around large underground cavern based on numerical analysis: A case study in the Cai Mep project. *Journal of Mining and Earth Sciences*, *63*(3), 50–58. https://doi.org/10.46326/JMES.2022.63(3a).06

Warpinski, N. (2009). Microseismic monitoring: Inside and out. *Journal of Petroleum Technology*, *61*(11), 80–85. https://doi.org/10.2118/118537-JPT

Xu, Q., Chen, J.-T., & Xiao, M. (2020). Analysis of unsteady seepage field and surrounding rock stability of underground cavern excavation. *Tunnelling and Underground Space Technology*, *97*, Article 103239. https://doi.org/10.1016/j.tust.2019.103239

Yan, H.-C., Liu, H.-Z., Li, Y., Zhuo, L., Xiao, M.-L., Chen, K.-P., Wu, J.-M., & Pei, J.-L. (2023). Inversion analysis of the in situ stress field around underground caverns based on particle swarm optimization optimized back propagation neural network. *Applied Sciences*, *13*(8), Article 4697. https://doi.org/10.3390/app13084697

Yu, J., Meng, X., Yan, B., Xu, B., Fan, Q., & Xie, Y. (2020). Global navigation satellite system-based positioning technology for structural health monitoring: a review. *Structural Control and Health Monitoring*, *27*(1), Article e2467. https://doi.org/10.1002/stc.2467

Zhang, Q., Li, F., Duan, K., Yu, G., Cheng, L., & Guo, X. (2021). Experimental investigation on splitting failure of high sidewall cavern under three-dimensional high in-situ stress. *Tunnelling and Underground Space Technology*, *108*, Article 103725. https://doi.org/10.1016/j.tust.2020.103725

Zhao, B.-x., Wang, Z.-g., Liu, R., & Lei, L.-q. (2014). Review of microseismic monitoring technology research. *Progress in Geophysics*, *29*(4), 1882–1888.

Zheng, X., Zhou, J., Wang, F., & Chen, Y. (2018). Routes to failure and prevention recommendations in work systems of hydropower construction. *Journal of Civil Engineering and Management*, *24*(3), 206–222. https://doi.org/10.3846/jcem.2018.1647